

Photoprocesses in protoplanetary disks

Ewine F. van Dishoeck,^a Bastiaan Jonkheid^a
and Marc C. van Hemert^b

^a Leiden Observatory, P.O. Box 9513, 2300 RA Leiden, The Netherlands.
E-mail: ewine@strw.leidenuniv.nl

^b Leiden Institute of Chemistry, P.O. Box 9502,
2300 RA Leiden, The Netherlands

November 11, 2018

Circumstellar disks are exposed to intense ultraviolet (UV) radiation from the young star. In the inner disks, the UV radiation can be enhanced by more than seven orders of magnitude compared with the average interstellar radiation field, resulting in a physical and chemical structure that resembles that of a dense photon-dominated region (PDR). This intense UV field affects the chemistry, the vertical structure of the disk, and the gas temperature, especially in the surface layers. The parameters which make disks different from more traditional PDRs are discussed, including the shape of the UV radiation field, grain growth, the absence of PAHs, the gas/dust ratio and the presence of inner holes. Illustrative infrared spectra from the Spitzer Space Telescope are shown. New photodissociation cross sections for selected species, including simple ions, are presented. Also, a summary of cross sections at the Lyman α 1216 Å line, known to be strong for some T Tauri stars, is made. Photodissociation and ionization rates are computed for different radiation fields with color temperatures ranging from 30000 to 4000 K and grain sizes up to a few μm . The importance of a proper treatment of the photoprocesses is illustrated for the transitional disk toward HD 141569A which includes grain growth.

1 Introduction

It is well established observationally and theoretically that many young stars in the solar neighborhood are surrounded by disks, i.e., flattened rotating concentrations of gas and dust (see [18] for a review). In the early phases, up to a few Myr after collapse of the parent cloud,

the disks are rich in gas and dust inherited from the cloud core. Once accretion onto the star stops and the disk becomes less turbulent, the $\sim 0.1 \mu\text{m}$ interstellar grains coagulate to larger and larger particles and settle to the midplane, eventually forming km-sized planetesimals which interact gravitationally to form protoplanets (e.g., [80]). In this period, between a few and 10 Myr, also most of the gas may be dissipated from the disk although the precise time scale for gas removal is still uncertain. Dust disks are observed around much older (up to a few Gyr) stars as well, but the grains in these disks are the ‘debris’ produced by collisions and fragmentation of planetesimals and are no longer the original interstellar particles (e.g., [37]). This paper is concerned with young, gas-rich disks up to the transitional stage when the disk becomes optically thin to UV radiation.

Young stars are known to be powerful emitters of UV radiation, with typical intensities at the disk surface that are orders of magnitude higher than the average interstellar radiation field [23]. For some sources, most of the flux may be contained in the Lyman α line [3]. These UV photons play a very important role in the physical and chemical structure of the disk, especially in the surface and intermediate layers. Many disks are thought to have a flaring structure, in which the disk height H and opening angle H/R increase with radius R (e.g., [7, 10]). In such a geometry the disk surface intercepts significantly more UV radiation from the star than in a flat geometry, heating the surface layers and increasing the scale height further when hydrostatic equilibrium is assumed in the vertical direction. Because the density in the upper layers is below that at which gas-grain coupling becomes effective, the gas temperature can be higher than the dust temperature due to photoelectric heating, affecting both the structure, chemistry and line formation [27, 29]. In the inner disk ($< 10\text{AU}$), the temperature can even become so high (several thousand K) that photoevaporation becomes effective [17].

The main effect of the UV radiation on the chemistry is through photodissociation and photoionization of molecules and atoms in the surface layers. These processes remain effective until most photons have been absorbed by the dust and the photorates have fallen below those of other chemical reactions, typically at a depth of a few magnitudes of extinction. The chemical structure of the outer disk has been modeled by various groups in both the radial and vertical direction (e.g., [82, 1, 47, 78]). In the vertical direction, the chemical structure resembles that of a photon-dominated region (PDR), with a transition from C^+ to C and CO around $A_V \approx 1$ mag and radicals such as CN and C_2H having a significant abundance in the intermediate layers. In the cold mid-plane ($< 20\text{K}$), most molecules are frozen out onto the grains. This layered chemical structure is consistent with observations of ions and radicals with abundance ratios that are similar or higher than those found in PDRs (e.g., [14, 70]). If the UV radiation is energetic enough to dissociate CO, isotope selective processes may occur leading to fractionation of CO isotopes which can eventually be incorporated into meteorites [46]. Finally, UV photons can affect the chemistry through photodesorption of ices brought to the surface by vertical mixing in the disk [82].

The above discussion illustrates the need for accurate photodissociation cross sections to de-

scribe the disk chemistry. In this paper, photodissociation rates relevant for disks exposed to different types of radiation fields are presented, including calculations of cross sections for species not considered before. Also, a critical evaluation of available cross sections at the Lyman α wavelength is given. The resulting chemical structure is illustrated for the transitional disk around the Herbig Ae/Be star HD 141569A.

2 Photoprocesses in disks

The PDR structure of a disk differs from that of the more commonly studied PDRs in molecular clouds [24]. First, the spectral shape of the stellar radiation field can differ significantly from that of the standard interstellar radiation field (ISRF), especially for the cooler T Tauri stars. Figure 1 compares the standard ISRF cf. [12] with that of a 10000 K (typical Herbig Ae star) and a 4000 K (typical T Tauri star) radiation field, normalized to have the same integrated intensity from 912–2050 Å. Below 2000 Å where most molecules are photodissociated, the 4000 K field has orders of magnitude lower intensity. The figure also includes a NEXTGEN simulated spectrum of a B9.5 star [22], illustrating that the intensity may be further reduced by stellar absorption lines in the critical 912–1100 Å where H₂ and CO are photodissociated. These stellar lines become increasingly important at lower stellar temperatures. Some T Tauri stars are known to have excess UV emission above that of a 4000 K blackbody, either from a hot boundary layer between the accretion disk and the star or from chromospheric stellar activity, bringing the overall shape back closer to that of the ISRF [6, 30]. Specific resonance lines like Lyman α can dominate the spectrum [3]. The key chemical effect is that H₂ and CO are hardly photodissociated by ‘cool’ stars at 912–1100 Å; only the general ISRF incident on the disk sets up the H \rightarrow H₂ and C⁺ \rightarrow C \rightarrow CO transitions [78]. Other molecules with photodissociation channels primarily at short wavelengths (e.g., N₂, CN) are equally affected.

Second, the UV field can be orders of magnitude higher than that studied in molecular clouds. For example, at 15 AU from an A0 star, the radiation is 10⁷ times that of the ISRF. For such high fluxes, photorates can become comparable to dissociative recombination rates so that photodissociation of ions needs to be included in the models.

Third, the grain sizes and properties may be very different from those found in clouds. In particular, there is strong evidence from infrared observations that grains in the upper disk layers have grown from $\sim 0.1 \mu\text{m}$ to a few μm in size regardless of the spectral type of the star (e.g., [71, 32]). Figure 2 illustrates this growth using recent Spitzer Space Telescope spectra of the 10 and 20 μm silicate feature. Larger grains have significantly lower extinction at UV wavelengths. Also, PAHs may have lower abundances and are detected toward only few T Tauri stars [16].

Fourth, the gas/dust mass ratio can differ from the interstellar medium value of 100. Currently, it is unclear whether the (small) dust particles disappear before the gas or vice versa. However,

dust-free gaps, rings and holes in disks have been found for some objects including the HD 141569A disk (e.g., [2, 8]). Some remaining gas can be present in these dust holes (e.g., [50]). Fifth, the density in the disk PDR varies by orders of magnitude, both in vertical and radial direction, in contrast with the near constant density assumed for clouds. If ices are released into the gas due to vertical mixing followed by thermal or photodesorption, the initial conditions for the PDR are different from those of standard clouds. For example, the presence of enhanced gaseous H₂O has been shown to modify the PDR chemistry for the case of protostellar envelopes [62].

Finally, young stars are known to be powerful X-ray emitters (e.g., [15]). In addition to direct ionization, the UV radiation resulting from the interaction of the secondary electrons with H₂ has a major effect on the chemistry [19, 63]. This spectrum consists of many discrete lines originating from the H₂ B and C electronic states, with peaks at 1500–1600 Å and shorter wavelengths. Thus, many of the basic photodissociation processes discussed here are also relevant for models which take X-rays into account.

3 Photodissociation cross sections and rates

The photodissociation rate of a molecule can be computed from

$$k_{pd}^{cont} = \int \sigma(\lambda) I(\lambda) d\lambda \quad \text{s}^{-1} \quad (1)$$

where σ is the photodissociation cross section in cm² and I is the mean intensity of the radiation in photons cm⁻² s⁻¹ Å⁻¹. Usually σ is a broad, continuous function with wavelength peaking close to the vertical excitation energy of the electronic state involved in the process. For photodissociation initiated by line absorptions (e.g., predissociation), the rate becomes

$$k_{pd}^{line} = \frac{\pi e^2}{mc^2} \lambda_{ul}^2 f_{ul} \eta_u I_{ul} \quad \text{s}^{-1} \quad (2)$$

where f_{ul} is the oscillator strength for absorption from lower level ℓ to upper level u and η_u the dissociation efficiency of state u , which lies between 0 and 1. The numerical value of the factor $\pi e^2/mc^2$ is 8.85×10^{-21} in the adopted units with λ in Å. The total photodissociation rate of a molecule is obtained by summing over all channels.

Overviews of photodissociation cross sections and interstellar photodissociation rates of astrophysically relevant molecules have been given by [40, 73, 57, 26]. Data on cross sections can be found in the chemical physics literature, either from experiments (stable molecules) or theory (radicals, ions). These summaries include only limited data on the photodissociation of small ions which are key to building carbon- and oxygen species. Therefore, a literature search was performed and new cross sections were calculated for several species. Also, the first critical evaluation of cross sections at the Lyman α wavelength is presented. Finally, photodissociation rates are calculated for different radiation fields and grain parameters.

3.1 New photodissociation cross sections

For small molecules and ions, quantum chemical calculations of the potential energy curves and transition dipole moments combined with dynamical calculations of the nuclear motions can provide accurate photodissociation cross sections and oscillator strengths (see [34] for review). All new calculations presented here were performed with the MOLPRO set of programs [81], using the VTZ atomic orbital basis set [13]. For neutral molecules, diffuse s and p functions were added to allow for a proper description of molecular Rydberg states. Molecular orbitals were generated in state-averaged complete active space (CAS) calculations. In the ultimate contracted multi-reference configuration-interaction (CI) calculation, typically 50 reference configurations per symmetry were used. Thus, around 100000 contracted configurations out of 300000 uncontracted configurations were generated per symmetry. Orbitals with an orbital energy below -15 eV were kept doubly occupied in all CI calculations.

Typically, the lowest 5 electronic states of each symmetry were calculated at the ground-state equilibrium geometry together with the corresponding transition moments. For diatomics, complete potential energy curves were computed as well. Many of the excited states are bound and the predissociation efficiencies are often unknown. In the following, individual cases are discussed in more detail.

CH₂⁺: Accurate CI calculations by Theodorakopoulos & Petsalakis [69] show many dipole-allowed excited states below 13.6 eV. Their 1, 2 and 3²B₂, 2, 3 and 4 ²A₁ and 2²B₁ states have been included with $f=0.008, 0.0001, 0.02, 0.01, 0.06, 0.05$ and 0.03 , respectively.

CH₄⁺: Detailed studies of the CH₄⁺ photodissociation processes starting from its lowest C_{2v} state have been carried out by van Dishoeck et al. [76] indicating that the higher excited states are likely dissociative. The oscillator strengths into the 2, 3 ²A₁ and 2²B₁ states computed in this work are $f=0.04, 0.04$ and 0.08 , respectively.

O₂⁺: Calculations show that all electronic states below 13.6 eV are bound [25]. Our computed oscillator strengths to the A²Π_u and 2²Π_u states—the only dipole allowed states below 13.6 eV and above the dissociation limit—are only $f=0.005$ each.

CO⁺: CO⁺ is strongly bound with a dissociation energy of 8.34 eV, but its higher excited D²Π, G, E and F ²Σ⁺ states are likely (pre-)dissociative [38]. The calculated oscillator strengths to the D and G states are $f=0.01$ and 0.02 , respectively. Similar values have been assumed for the higher states.

HCO⁺: The excited electronic states and photodissociation processes of HCO⁺ have been studied in detail by Koch et al. [35, 36]. HCO⁺ is remarkably transparent at UV wavelengths: the only dipole-allowed dissociative state is the 1¹Π state around 11.5 eV with a small cross section.

H₂O⁺: Calculations show that there are no dipole-allowed dissociative electronic states below 13.6 eV so that the interstellar H₂O⁺ photodissociation rate is negligible.

SiO: The electronic structure of SiO is similar to that of CO, but with a lower dissociation

energy of 8.26 eV implying that even the lower Rydberg states can contribute to SiO photodissociation if they are fully predissociated. Our computed oscillator strengths to the $3\ ^1\Sigma^+$ and $2, 3, 4$ and $5\ ^1\Pi$ states are $f=0.10, 0.32, 0.03, 0.11$ and 0.10 , respectively.

3.2 Lyman α cross sections

The Lyman α line can outshine the continuum radiation, so that it is important to know whether a molecule can be photodissociated at 1216 Å or not. Table 1 summarizes the cross sections for a number of key molecules, including those that are known to have significant abundances in the inner disk [47]. The table contains references to the original experimental or theoretical work as well as an assessment of the accuracy of the data, with the notation A (σ known to better than 50%), B (σ uncertain up to a factor of two) or C (σ uncertain up to an order of magnitude).

The following molecules cannot be dissociated by Lyman α radiation: H_2 , CO, N_2 , CN, H_3^+ , OH^+ , H_2O^+ and HCO^+ . An interesting case is formed by O_2 . The absorption cross section at 1215–1216 Å is known to be small, of order $(1 - 2) \times 10^{-20}$ cm² [53], but there are resonances into the $v' = 0$ and 1 levels of the $2\ ^3\Sigma_u^-$ state at 1245 and 1205 Å, with $f = 0.015$ each [5]. If the Lyman α line is as wide as observed for some stars (1205–1230 Å, ± 0.1 eV [3]), these states can make a small contribution.

Experimentally determined cross sections at Lyman α are generally accurate to better than a factor of 2, especially when the absorption is continuous. For molecules for which only theoretical calculations are available (e.g., CH, CH_2 , C_2H , C_3 , ...), the cross sections at Lyman α are highly uncertain because the energy level calculations are uncertain by ~ 0.2 eV, which is not accurate enough to determine whether there is an exact resonance of a predissociative state at 1216 Å. For continuous absorption into a directly repulsive state around 10.2 eV (e.g., OH), the computed results are reliable, however. For some molecules, no estimate is possible because of lack of both experimental and theoretical data around Lyman α . This includes C_3H_2 , SH, SH^+ , CS and SiO.

Only a few molecules can be photoionized by Lyman α (see Table 2 of [73] for ionization potentials). For species like NH_3 and NO, the photoionization cross sections or yields have been measured so that the dissociation and ionization parts can be separated. In other cases such as CH_3 , the branching ratio is unknown. SO has an ionization potential of 10.29 eV, just above the Lyman α threshold, whereas CS_2 has 10.08 eV, just below. Of the major atoms, C, N, O, and S cannot be photoionized by Lyman α whereas Mg, Si and Fe can.

3.3 Photodissociation rates for Herbig Ae and T Tauri stars

The database on photodissociation and ionization cross sections assembled by van Dishoeck [73] has been used together with the above new input to compute photodissociation rates for

various radiation fields. No attempt has been made to systematically review the chemical physics literature since 1988 for molecules other than those discussed in §3.1. Minor updates are included for some species such as CH₂, for which the cross sections of [77] are adopted. References to the sources for the cross sections are given in Table 1 of [73], which also includes the most likely dissociation products. The resulting rates for the standard ISRF cf. [12] are given in Tables 2 and 3.

In calculating the photodissociation rates, it has been assumed that all states above the dissociation limit have 100% dissociation efficiency, thus providing a maximum value ($\eta_u = 1$). Even with this assumption, the photodissociation of ions is on average significantly slower than that of neutrals. Several ions (e.g., H₃⁺, H₂O⁺) do not even have any dipole-allowed dissociative electronic transitions below 13.6 eV. Note that CH⁺ dissociates primarily into C + H⁺ for the radiation fields considered here, not C⁺ + H as listed in UMIST99. In contrast, OH⁺ dissociates primarily into O⁺ + H.

The photodissociation rates for larger molecules are uncertain because experimental data are sparse and incomplete. Moreover, often only absorption cross sections are known, not the dissociation yields. For large molecules, absorption is followed by internal conversion to highly excited vibrational levels of the ground electronic state, only some of which lead to dissociation. Also, the products of the photodissociation are largely unknown and can vary with wavelength; see [48] for an illustrative example for the case of CH₃OH.

Tables 2 and 3 include the photodissociation and photoionization rates for a $T_{BB} = 10000$ K and a 4000 K blackbody radiation field. As noted in §2, the shapes of the UV fields of Herbig Ae and T Tauri stars are thought to lie in between these three extremes. Their intensities have been normalized such that the integrated values from 912–2050 Å are the same as those of the Draine [12] field, 2.67×10^{-3} erg cm⁻² s⁻¹. The latter value is a factor of 1.7 larger than that of the integrated Habing [21] field of 1.6×10^{-3} erg cm⁻² s⁻¹ used in other normalizations. The adopted dilution factors are 1.57×10^{-14} and 1.90×10^{-9} for 10000 and 4000 K, respectively. For applications in disk chemistry, these rates need to be scaled to the appropriate strength at a certain distance from the star. The photorates for (scaled) fields with $T_{BB} = 20000 - 30000$ K are close to those for the ISRF.

As shown previously for interstellar clouds exposed to cool stars [61], the photorates can decrease by orders of magnitude if a 4000 K blackbody is used. Species like H₂, CO, C, CN and N₂, which are only dissociated or ionized at <1100 Å, are most affected (cf. Figure 1): their photorates become negligible for $T_{BB} = 4000$ K. In contrast, molecules with dissociation channels at wavelengths as long as 3000 Å (e.g., CH, HCO, O₃) can have enhanced rates in the cooler fields with the adopted normalization. Molecules which absorb over a broad wavelength range (e.g., OH, H₂O, NO) vary by only a factor of a few between $T_{BB} = 30000$ and 4000 K.

Illustrative examples of the effect of Lyman α radiation on the photorates in disks are given by [3]. The photodissociation and ionization efficiencies corresponding to Lyman α absorption in the context of X-ray induced chemistry are summarized by [44] for selected species.

3.4 Depth-dependence of photorates

With depth into a cloud or disk, the UV radiation is attenuated due to absorption and scattering by dust grains [56]. For typical $0.1 \mu\text{m}$ interstellar grains, the extinction, albedo and scattering phase function are taken from [57]. The rates are then fitted to a single exponential decay with

$$k_{pd} = k_{pd}^o \exp(-\gamma A_V) \text{ s}^{-1}. \quad (3)$$

The fits of γ are performed over the range $A_V = 0 - 3$ mag and are appropriate for a model in which the radiation is incident from one side only. The absolute values of γ vary by $\sim 10\%$ depending on the extinction range chosen for the fits; the relative values from molecule to molecule are more accurate. Tables 2 and 3 contain the results for the different radiation fields. The values of γ for the ISRF differ from those of van Dishoeck [73] due to the adopted grain properties, which are in between those of grain models 2 and 3 of [56] used previously. Interestingly, the values of γ do not change dramatically with T_{BB} for most species, even though there is a general trend for γ to become smaller with cooler fields (see also [61]).

When grains grow larger, the main effect on the grain parameters is the smaller extinction at UV wavelengths, which becomes comparable to that at visible wavelengths (e.g., [59]). The photorates have been re-computed as a function of depth using the properties for μm -sized ice-coated grains derived for the HD 141569A disk [45, 28]. For species such as C and CO which absorb only at the shortest wavelengths, the exponents γ are lowered from > 3 to ~ 0.6 for the ISRF. For molecules which are dissociated primarily at long wavelengths (e.g., HCO), γ is lowered from 1.1 to 0.47. Other species have exponents γ in between these two values. For $T_{BB} = 4000$ K, the trends are similar, with values of γ between 0.6 and 0.38. Thus, the differences between molecules in the depth dependence of the photorates are minimized for large grains.

4 A disk model example

In this work, the effects of different radiation fields and different grain properties are taken into account explicitly by calculating at each point in the disk the UV radiation field from the star as well as the ISRF (either in 1+1D or in full 2D) and then computing the photodissociation rates by integrating the cross sections multiplied by the radiation intensity over wavelength [78, 28]. Self-shielding of H_2 and CO as well as mutual shielding of CO and its isotopes are included. X-rays are not included, nor is time-dependence, vertical mixing or photodesorption of ices.

As an example, the disk around the Herbig Ae/Be star HD 141569A (B9.5 V, $22 L_\odot$, 99 pc) is modelled. This ~ 5 Myr old star has a large ~ 500 AU disk with a huge inner hole in the dust out to 150 AU and two dust rings at 185 and 325 AU seen in scattered light images (e.g.,

[2, 8]*). The outer rings may be explained by tidal interactions with two M-type companions, HD 141569B and C, but other explanations such as a giant planet are not excluded. The origin of the inner hole is unknown. The disk is optically thin to UV continuum radiation and the grains have grown to at least μm size [45]. Nevertheless, gas is still present since the CO $J=2-1$ and $3-2$ millimeter [11] and the $v = 1 - 0$ infrared [4] lines have been detected. Moreover, PAHs have been seen, albeit at a low level [68]. Thus, this disk provides a good opportunity to investigate the effects of different UV radiation fields and larger grains.

Detailed models to constrain the total gas mass in this disk have been developed by Jonkheid et al. [28]. They use a 1+1D approach, with 1D PDRs computed in the radial rather than vertical direction for this optically thin disk. Both the radiation from the star (see Figure 1) and the ISRF are included. The size of the dust grains enters the chemistry in various ways: in the UV extinction, in the H_2 formation rate, and through the photoelectric heating efficiency [31]. The best-fitting model to the CO millimeter lines has a total gas mass of $80 M_{\text{Earth}}$, compared with a total dust mass of $2.2 M_{\text{Earth}}$ in grains up to 1 cm. An important conclusion is that some gas must be present in the inner hole to provide sufficient H_2 and CO self-shielding in the radial direction. The PAH abundance with respect to total hydrogen is $\sim 10^{-10}$, but even at this low abundance PAHs are an important site for H_2 formation. Models without PAHs require much larger gas masses [28].

Figures 3 and 4 present the radial and vertical distributions of various molecules in the HD 141569A disk, both with and without the ISRF. Because the stellar radiation field has few photons at wavelengths below 1200 \AA , the photodissociation of CO and H_2 and photoionization of C occurs mostly by the ISRF in the outer disk. The vertical slices show the typical PDR structure with atomic H and C^+ dominant on the surface, and the transition to H_2 taking place in the intermediate layer. However, the CO column never becomes large enough in the vertical direction for significant self-shielding so that carbon stays in atomic form. Other molecules like CH and C_2H which are not self-shielding and can photodissociate over a large wavelength range continue to be dissociated very rapidly by the stellar radiation. Thus, even without the ISRF, the CO abundance stays low since its precursor molecules have very low abundances. Neutral atomic carbon is the dominant form of carbon since there are few ionizing photons. The predicted peak line intensity of $\sim 1 \text{ K}$ should be readily detectable by submillimeter telescopes [28]. Failure to detect this line may imply that the observed CO is not a relic of the interstellar cloud from which HD 141569A formed.

5 Conclusions

The main results of this work are as follows.

*see <http://hubblesite.org/newscenter/newsdesk/archive/releases/2003/02/> for image

- New photodissociation cross sections are presented for several species not considered before. Also, the first critical evaluation of cross sections at Lyman α is given.
- The photodissociation of ions is potentially important in (inner) disk chemistry where the radiation field can be 10^7 times more intense than the standard ISRF. However, the photorates of many ions, especially those containing oxygen, are found to be slow compared with those of neutrals.
- Photorates have been computed for a range of radiation fields appropriate for Herbig Ae/Be and T Tauri stars. Molecules such as H_2 , CO, N_2 and CN, which are photodissociated only below 1200 Å, have rates that are more than 5 orders of magnitude decreased for a $T_{BB} = 4000$ K blackbody field.
- The exponent γ characterizing the depth-dependence of the photorates decreases with T_{BB} but the effect is not large in the 4000–30000 K range for most species. For larger μm -sized grains, the depth dependence of the photorates becomes much shallower, with γ falling in a narrow range of 0.4–0.6 for all species.
- The example of the HD 141569A disk illustrates that both the shape of the stellar radiation field and the size of the grains affect the chemistry. Both need to be treated correctly to derive quantitative conclusions about the gas mass and chemistry from observed lines. Even a small amount of PAHs or small grains can significantly affect dissociation and ionization rates, as well as the H_2 formation rate.

6 Acknowledgments

We are grateful to the Spitzer ‘Cores to Disks’ team, in particular J. Kessler-Silacci and V. Geers, for providing observational data. The HD 141569A modeling is performed in collaboration with J.C. Augereau and I. Kamp. Astrochemistry in Leiden is supported by a Spinoza grant from the Netherlands Organization for Scientific Research (NWO).

References

- [1] Y. Aikawa, G.J. van Zadelhoff, E.F. van Dishoeck and E. Herbst, *Astron. Ap.*, 2002, **386**, 622
- [2] J. Augereau, A. Lagrange, D. Mouillet and F. Ménard, *Astron. Ap.*, 1999, **350**, L51
- [3] E. Bergin, N. Calvet, P. D'Alessio, G.J. Herczeg, *Astrophys. J.*, 2003, **591**, L159
- [4] S. Brittain, T. Rettig, T. Simon, et al., *Astrophys. J.*, 2003, **588**, 535
- [5] R.J. Buenker, S.D. Peyerimhoff and M. Perić, *Chem. Phys. Lett.*, 1976, **42**, 383
- [6] N. Calvet and E. Gullbring, *Astrophys. J.*, 1998, **509**, 802
- [7] E.I. Chiang and P. Goldreich, *Astrophys. J.*, 1997, **490**, 368
- [8] M. Clampin, J.E. Krist, D.R. Ardila, et al. *Astron. J.*, 2003, **123**, 385
- [9] R.E. Connors, J.L. Roebber and K. Weiss, *J. Chem. Phys.*, 1974, **60**, 5011
- [10] P. D'Alessio, J. Cantó, N. Calvet and S. Lizano, *Astrophys. J.*, 1998, **500**, 411
- [11] W. Dent, J. Greaves and I. Coulson, *Mon. Not. R. Astr. Soc.*, 2005, **359**, 663
- [12] B.T. Draine, *Astrophys. J. Suppl.*, 1978, **36**, 595
- [13] T. Dunning, *J. Chem. Phys.*, 1971, **55**, 716
- [14] A. Dutrey, S. Guilloteau and M. Guélin, *Astron. Ap.*, 1997, **317**, L55
- [15] E.D. Feigelson and Th. Montmerle, *Ann. Rev. Astron. Ap.*, 1999, **37**, 363
- [16] V.C. Geers, et al., *Astron. Ap.*, 2006, submitted
- [17] U. Gorti and D.J. Hollenbach, *Astrophys. J.*, 2004, **613**, 424
- [18] J.S. Greaves, *Science*, 2005, **307**, 68
- [19] R. Gredel, S. Lepp, A. Dalgarno and E. Herbst, *Astrophys. J.*, **347**, 289
- [20] J.A. Guest and L.C. Lee, *J. Phys. B*, 1981, **14**, 3401
- [21] H.J. Habing, *Bul. Astr. Inst. Neth.*, 1968, **19**, 421
- [22] P. Hauschildt, F. Allard and E. Baron, *Astrophys. J.*, 1999, **512**, 377

- [23] G.H. Herbig and R.W. Goodrich, *Astrophys. J.*, 1986, **309**, 294
- [24] D.J. Hollenbach and A.G.G.M. Tielens, *Ann. Rev. Astron. Ap.*, 1997, **35**, 179
- [25] N. Honjou, K. Tanaka, K. Ohno, H. Taketa, *Mol. Phys.*, 1978, **35**, 1569
- [26] W.F. Huebner, J.J. Keady and S.P. Lyon, *Astrophys. Sp. Sci.*, 1992, **195**, 1
- [27] B. Jonkheid, F.G.A. Faas, G.-J. van Zadelhoff and E.F. van Dishoeck, *Astron. Ap.*, 2004, **428**, 511
- [28] B. Jonkheid, I. Kamp, J.C. Augereau and E.F. van Dishoeck, *Astron. Ap.*, 2006, submitted
- [29] I. Kamp and C.P. Dullemond, *Astrophys. J.*, 2004, **615**, 991
- [30] I. Kamp and F. Sammar, *Astron. Ap.*, **427**, 561
- [31] I. Kamp and G.J. van Zadelhoff, *Astron. Ap.*, 2001, **373**, 641
- [32] J. Kessler-Silacci et al., *Astrophys. J.*, 2006, in press
- [33] K.P. Kirby and E.M. Goldfield, *J. Chem. Phys.*, 1991, **94**, 1271
- [34] K.P. Kirby and E.F. van Dishoeck, *Adv. At. Mol. Phys.*, 1988, **25**, 437
- [35] A. Koch, E.F. van Dishoeck and M.C. van Hemert, *Ber. Bunsenges. Phys. Chem.*, 1995, **99**, 393.
- [36] A. Koch, M.C. van Hemert and E.F. van Dishoeck, *J. Chem. Phys.*, 1995, **103**, 7006.
- [37] A.-M. Lagrange, D.E. Backman, P. Artymowicz, *Protostars & Planets IV*, 2000, eds. V. Mannings et al. (Tucson: Univ. of Arizona), p. 639
- [38] H. Lavendy, J.M. Robbe and J.P. Flament, *Chem. Phys. Lett.*, 1993, **205**, 456
- [39] L.C. Lee, *J. Chem. Phys.*, 1980, **72**, 6414
- [40] L.C. Lee, *Astrophys. J.*, 1984, **282**, 172
- [41] L.C. Lee and C.C. Chiang, *J. Chem. Phys.*, 1983, **78**, 688
- [42] L.C. Lee and M. Suto, *Chem. Phys.*, 1986, **110**, 161
- [43] L.C. Lee, X. Wang and M. Suto, *J. Chem. Phys.*, 1987, **86**, 4353
- [44] S. Lepp and A. Dalgarno, *Astron. Ap.*, 1996, **306**, L21

- [45] A. Li and J.I. Lunine, *Astrophys. J.*, 2003, **594**, 987
- [46] J.R. Lyons and E.D. Young, *Nature*, 2005, **435**, 317
- [47] A.J. Markwick, M. Ilgner, T.J. Millar and Th. Henning, *Astron. Ap.*, 2002, **385**, 632
- [48] T.J. Millar, in *Astrochemistry across the Universe*, 2006, IAU Symposium 231, ed. D. Lis, E. Herbst and G.A. Blake (Cambridge: CUP), in press
- [49] M. Min, J.W. Hovenier and A. de Koter, *Astron. Ap.*, 2005, **432**, 909
- [50] J. Muzerolle, N. Calvet, L. Hartmann and P. d'Alessio, *Astrophys. J.*, 2003, **597**, L149
- [51] J.B. Nee and L.C. Lee, *J. Chem. Phys.*, 1986, **84**, 5303
- [52] J.B. Nee, M. Suto and L.C. Lee, *Chem. Phys.*, 1985, **98**, 147
- [53] S. Ogawa and M. Ogawa, *Can. J. Phys.*, 1975, **53**, 1845
- [54] H. Okabe, *J. Chem. Phys.*, 1981, **75**, 2772
- [55] B. Pouilly, J.M. Robbe, J. Schamps and E. Roueff, *J. Phys. B*, 1983, **16**, 437
- [56] W.G. Roberge, A. Dalgarno and B.P. Flannery, *Astrophys. J.*, 1981, **243**, 816
- [57] W.G. Roberge, D. Jones, S. Lepp and A. Dalgarno, *Astrophys. J. Suppl.*, 1991, **77**, 287
- [58] J. Römel, S.D. Peyerimhoff and R.J. Buenker, *Chem. Phys. Lett.*, 1978, **58**, 1
- [59] C.J. Shen, J.M. Greenberg, W.A. Schutte and E.F. van Dishoeck, *Astron. Ap.*, 2004, **415**, 203
- [60] S. Shih, S.D. Peyerimhoff and R.J. Buenker, *J. Mol. Spectr.*, 1979, **74**, 124
- [61] M. Spaans, A.G.G.M. Tielens, E.F. van Dishoeck and E.L.O. Bakes, *Astrophys. J.*, 1994, **437**, 270
- [62] P. Stäuber, S.D. Doty, E.F. van Dishoeck, J.K. Jørgensen and A.O. Benz, *Astron. Ap.*, 2004, **425**, 577
- [63] P. Stäuber, S.D. Doty, E.F. van Dishoeck and A.O. Benz, *Astron. Ap.*, 2005, **440**, 949
- [64] M. Suto and L.C. Lee, *J. Chem. Phys.*, 1983, **78**, 4515
- [65] M. Suto and L.C. Lee, *J. Chem. Phys.*, 1984, **80**, 4824

- [66] M. Suto and L.C. Lee, *J. Geophys. Res.*, 1985, **90**, 13037
- [67] M. Suto, X. Wang and L.C. Lee, *J. Chem. Phys.*, 1986, **85**, 4228
- [68] R. Sylvester, C. Skinner, M. Barlow and V. Mannings, *Mon. Not. R. Astron. Soc.*, 1996, **279**, 915
- [69] G. Theodorakopoulos and I.D. Petsalakis, *J. Mol. Struct.*, 1991, **230**, 205
- [70] W.-F. Thi, G.-J. van Zadelhoff and E.F. van Dishoeck, *Astron. Ap.*, 2004, **425**, 955
- [71] R. van Boekel, M. Min, L.B.F.M. Waters, A. de Koter, C. Dominik, M.E. van den Ancker, and J. Bouwman, *Astron. Ap.*, 2005, **437**, 189
- [72] E.F. van Dishoeck, *J. Chem. Phys.*, 1987, **86**, 196
- [73] E.F. van Dishoeck, in *Rate coefficients in Astrochemistry*, 1988, ed. T.J. Millar & D.A. Williams (Dordrecht: Kluwer), 49
- [74] E.F. van Dishoeck and J.H. Black, *Astrophys. J.*, 1982, **258**, 533
- [75] E.F. van Dishoeck and A. Dalgarno, *Icarus*, 1984, **59**, 305
- [76] E.F. van Dishoeck, W.J. van der Hart and M. van Hemert, *Chem. Phys.*, 1980, **50**, 45
- [77] E.F. van Dishoeck, R.A. Bearda and M.C. van Hemert, *Astron. Ap.*, 1996, **307**, 645
- [78] G.-J. van Zadelhoff, Y. Aikawa, M.R. Hogerheijde and E.F. van Dishoeck, *Astron. Ap.*, 2003, **397**, 789
- [79] K. Watanabe and S.P. Sood, *Sci. Light*, 1965, **14**, 36
- [80] S.J. Weidenschilling, *Icarus*, 1997, **127**, 290
- [81] H.-J. Werner et al., MOLPRO 2002.6 (Birmingham: Univ.Birmingham), 2003
www.molpro.net
- [82] K. Willacy and W.D. Langer, *Astrophys. J.*, 2000, **544**, 903
- [83] K. Yoshino, J.R. Esmond, Y. Sun, W.H. Parkinson, K. Ito and T. Matsui, *J. Quant. Spect. Rad. Transf.*, 1996, **55**, 53

Table 1: Photodissociation and ionization cross sections at Lyman α 1216 Å^a

Species	σ_{pd} (cm ⁻²)	Accuracy ^b	Ref
CH	5.0(-20)	C	[72] T
CH ₂	5.0(-20)	C	[77] T
CH ₄	1.8(-17)	A	[41] E
C ₂	5.0(-18)	B	[55] T
C ₃	1.0(-18)	C	[58] T
C ₂ H	1.0(-18)	C	[60] T
C ₂ H ₂	≥4(-17) ^c	B	[65] E
C ₄ H ₂	3.5(-17)	B	[54] E
OH	1.8(-18)	B	[75] T
H ₂ O	1.2(-17)	A	[42] E
O ₂	1.0(-20) ^b	C	[53] E
CO ₂	6.1(-20)	A	[83] E
H ₂ CO	1.0(-17)	B	[67] E
CH ₃ OH	1.4(-17)	A	[52] E
NH	1.0(-18)	B	[33] T
NH ₃	1.0(-17)	A	[64] E
HCN	3.0(-17)	A	[39] E
HC ₃ N	2.5(-17)	B	[9] E
CH ₃ CN	2.0(-17)	A	[66] E
NO	4.0(-19)	B	[20] E
H ₂ S	3.3(-17)	B	[40] E
SO	1.0(-16)	C	[51] E
SO ₂	3.0(-17)	B	[40] E
OCS	1.5(-17)	A	[40] E
CS ₂	2.5(-17)	B	[40] E
Mg p.i.	3.0(-19)	A	[73]
Si p.i.	3.0(-17)	A	[73]
Fe p.i.	6.2(-19)	A	[73]
NH ₃ p.i.	2.0(-18)	B	[79] E
NO p.i.	1.6(-18)	B	[20] E
CS ₂ p.i.	2.0(-16)	B	[40] E

^a See text for list of species that cannot be dissociated or ionized by Lyman α

^b See text for discussion

^c $f=0.013$

Table 2: Photodissociation rates for various radiation fields^{a,b}

Species	k_{pd}^o (s ⁻¹)			γ		
	ISRF ^c	10000 K ^d	4000 K ^d	ISRF	10000 K	4000 K
H ₂ ⁺	5.7(-10)	1.9(-10)	2.9(-11)	2.37	2.14	1.99
CH	9.2(-10)	2.0(-9)	1.2(-7)	1.72	1.49	1.28
CH ⁺	3.3(-10)	3.5(-11)	4.8(-10)	2.94	1.78	1.31
CH ₂	5.8(-10)	1.2(-9)	2.1(-9)	2.02	2.02	2.12
CH ₂ ⁺	1.4(-10)	7.4(-11)	2.6(-11)	2.21	1.91	1.88
CH ₃	2.7(-10)	2.5(-10)	8.2(-10)	2.27	2.24	2.32
CH ₄	1.2(-9)	2.2(-10)	1.2(-12)	2.59	2.45	2.29
CH ₄ ⁺	2.8(-10)	4.2(-11)	1.3(-13)	2.71	2.58	2.48
C ₂	2.4(-10)	4.1(-11)	3.2(-13)	2.57	2.36	2.25
C ₂ H	5.2(-10)	1.9(-10)	7.2(-12)	2.30	2.16	2.10
C ₂ H ₂	3.3(-9)	1.2(-9)	1.3(-10)	2.27	2.12	1.97
C ₂ H ₄	3.0(-9)	2.2(-9)	5.2(-10)	2.10	1.96	1.90
C ₃	3.8(-9)	2.9(-9)	2.0(-10)	2.08	2.07	2.06
c-C ₃ H ₂	1.9(-9)	1.7(-9)	9.2(-10)	2.07	2.06	2.10
OH	3.9(-10)	1.8(-10)	1.3(-10)	2.24	2.00	1.67
OH ⁺	1.1(-11)	7.8(-13)	5.8(-13)	3.50	2.80	1.75
H ₂ O	8.0(-10)	4.3(-10)	1.2(-10)	2.20	1.97	1.90
O ₂	7.9(-10)	4.9(-10)	4.5(-11)	2.13	2.05	1.97
O ₂ ⁺	3.5(-11)	3.6(-11)	1.0(-11)	2.02	1.92	1.90
HO ₂	6.7(-10)	1.9(-9)	1.2(-8)	2.12	2.08	1.99
H ₂ O ₂	9.5(-10)	4.3(-10)	1.4(-10)	2.28	2.07	1.97
O ₃	1.9(-9)	5.4(-9)	1.5(-7)	1.85	1.69	1.57
CO	2.0(-10)	1.5(-11)	1.4(-15)	3.53	3.47	3.24
CO ⁺	1.0(-10)	2.2(-11)	1.2(-13)	2.52	2.43	2.32
CO ₂	8.9(-10)	9.0(-11)	1.2(-12)	3.00	2.53	2.00
HCO	1.1(-9)	2.5(-9)	3.5(-6)	1.09	1.09	0.81
HCO ⁺	5.4(-12)	4.5(-13)	7.9(-17)	3.32	3.32	3.32
H ₂ CO	1.0(-9)	6.7(-10)	1.8(-10)	2.16	1.99	1.90
CH ₃ OH	1.4(-9)	5.9(-10)	7.0(-11)	2.28	2.07	1.95

Table 3: Photodissociation rates for various radiation fields^{a,b} (Table 2 cont'd)

Species	k_{pd}^o (s ⁻¹)			γ		
	ISRF ^c	10000 K ^d	4000 K ^d	ISRF	10000 K	4000 K
NH	5.0(-10)	1.6(-10)	3.0(-12)	2.33	2.24	2.12
NH ⁺	5.4(-11)	1.8(-10)	8.4(-9)	1.64	1.52	1.51
NH ₂	7.5(-10)	1.0(-9)	5.7(-10)	2.00	1.90	1.89
NH ₃	1.2(-9)	1.0(-9)	1.1(-9)	2.12	1.99	2.00
N ₂	2.3(-10)	1.4(-11)	3.0(-16)	3.88	3.89	3.87
NO	4.7(-10)	4.3(-10)	2.9(-10)	2.12	1.96	1.94
NO ₂	1.4(-9)	1.0(-9)	3.4(-10)	2.12	1.97	1.92
N ₂ O	1.9(-9)	4.8(-10)	2.0(-11)	2.44	2.32	2.02
CN	2.9(-10)	2.1(-11)	2.0(-15)	3.54	3.49	3.23
HCN	1.6(-9)	2.5(-10)	3.7(-12)	2.69	2.44	2.02
HC ₃ N	5.6(-9)	3.0(-9)	2.5(-10)	2.16	2.12	2.12
CH ₃ CN	2.5(-9)	4.8(-10)	8.5(-12)	2.58	2.38	2.01
SH	9.8(-10)	1.3(-9)	1.6(-8)	2.04	1.85	1.34
SH ⁺	2.5(-10)	3.4(-10)	4.0(-8)	1.66	1.30	1.29
H ₂ S	3.1(-9)	2.0(-9)	3.2(-9)	2.27	2.12	2.16
CS	9.8(-10)	2.7(-10)	3.7(-12)	2.43	2.33	2.14
CS ₂	6.1(-9)	1.3(-8)	2.0(-8)	2.06	2.02	2.03
OCS	3.7(-9)	3.1(-9)	7.0(-10)	2.07	1.98	1.94
SO	4.2(-9)	4.4(-9)	9.4(-9)	2.37	2.18	2.16
SO ₂	1.9(-9)	7.4(-10)	2.8(-10)	2.38	2.11	1.94
SiH	2.8(-9)	1.4(-8)	8.0(-7)	1.59	1.55	1.22
SiH ⁺	2.7(-9)	1.0(-8)	3.3(-6)	1.21	1.13	1.11
SiO	1.6(-9)	5.6(-10)	9.9(-12)	2.28	2.21	2.19

^a See van Dishoeck [73] for products and references to cross section data

^b H₃⁺, HeH⁺ and H₂O⁺ cannot be photodissociated by radiation with $\lambda > 912$ Å, so $k_{pd}^o=0$

^c ISRF according to [12] with extension at >2000 Å of [74]

^d Scaled blackbody radiation field with temperature T_{BB} (see text)

Table 4: Photoionization rates for various radiation fields^a (Table 3)

Species	k_{pd}^o (s ⁻¹)			γ		
	ISRF ^b	10000 K ^c	4000 K ^c	ISRF	10000 K	4000 K
C	3.1(-10)	2.5(-11)	4.2(-15)	3.33	3.27	3.10
Mg	7.9(-11)	5.9(-11)	6.9(-12)	2.08	2.00	1.96
Si	3.1(-9)	1.2(-9)	4.1(-11)	2.27	2.17	2.09
S	6.0(-10)	5.9(-11)	4.0(-14)	3.08	2.95	2.76
Fe	2.8(-10)	1.3(-10)	5.8(-12)	2.20	2.14	2.05
CH	7.6(-10)	6.4(-11)	1.6(-14)	3.28	3.20	2.97
CH ₄	6.8(-12)	4.7(-13)	5.0(-18)	3.94	3.94	3.93
C ₂	4.1(-10)	2.6(-11)	1.0(-15)	3.81	3.81	3.78
C ₂ H ₂	3.3(-10)	2.4(-11)	2.4(-15)	3.52	3.49	3.33
C ₂ H ₄	4.1(-10)	3.5(-11)	1.1(-14)	3.21	3.11	2.91
C ₂ H ₆	2.3(-10)	1.5(-11)	7.6(-16)	3.74	3.73	3.55
O ₂	7.6(-11)	4.8(-12)	1.2(-16)	3.87	3.87	3.85
H ₂ O	3.1(-11)	2.0(-12)	3.6(-17)	3.90	3.90	3.88
NH ₃	2.8(-10)	2.6(-11)	1.1(-14)	3.12	3.04	2.86
NO	2.6(-10)	2.9(-11)	5.4(-14)	2.93	2.71	2.42
NO ₂	1.5(-10)	1.2(-11)	2.9(-15)	3.33	3.22	2.87
N ₂ O	1.7(-10)	1.1(-11)	1.4(-16)	3.93	3.93	3.92
H ₂ S	7.3(-10)	7.2(-11)	3.5(-14)	3.09	3.01	2.86
CS ₂	1.7(-9)	1.5(-10)	8.3(-14)	3.16	3.02	2.77
OCS	6.9(-10)	1.4(-11)	8.5(-15)	3.35	3.29	3.10
H ₂ CO	4.8(-10)	4.1(-11)	1.2(-14)	3.21	3.13	2.96

^a See van Dishoeck [73] for references to cross section data

^b See footnote *c* Table 2

^c See footnote *d* Table 2

- Fig. 1** Comparison of the interstellar radiation field (ISRF) according to [12] (with the extension by [74] for $>2000 \text{ \AA}$) with a 10000 K (dashed) and 4000 K (dotted) black-body scaled to have the same integrated intensity from 912–2050 \AA . The scaled NEXTGEN model radiation field a B9.5 star [22] (as appropriate for HD 141569A) is included as well (dash-dotted).
- Fig. 2** Evidence for grain growth in disks around T Tauri stars. Top: Spitzer Space Telescope observations of the 10 and 20 μm silicate Si-O stretching and O-Si-O bending mode features of two T Tauri stars, shifted by +0.4 and +0.2 for clarity. Bottom: normalized absorption efficiencies Q_{abs} for models of spherical amorphous olivines with various sizes, calculated using the distribution of hollow spheres (DHS) method of [49]. The models are offset by +0.4, +0.25 and +0.1, respectively. Figure based on [32].
- Fig. 3** Left: Radial distribution in the midplane of the HD 141569A disk of the temperature and density (top), and various chemical species (middle and bottom). Right: Vertical slice at $R = 300 \text{ AU}$. This model includes both the stellar radiation (Figure 1) and the ISRF.
- Fig. 4** As Figure 3, but without the ISRF

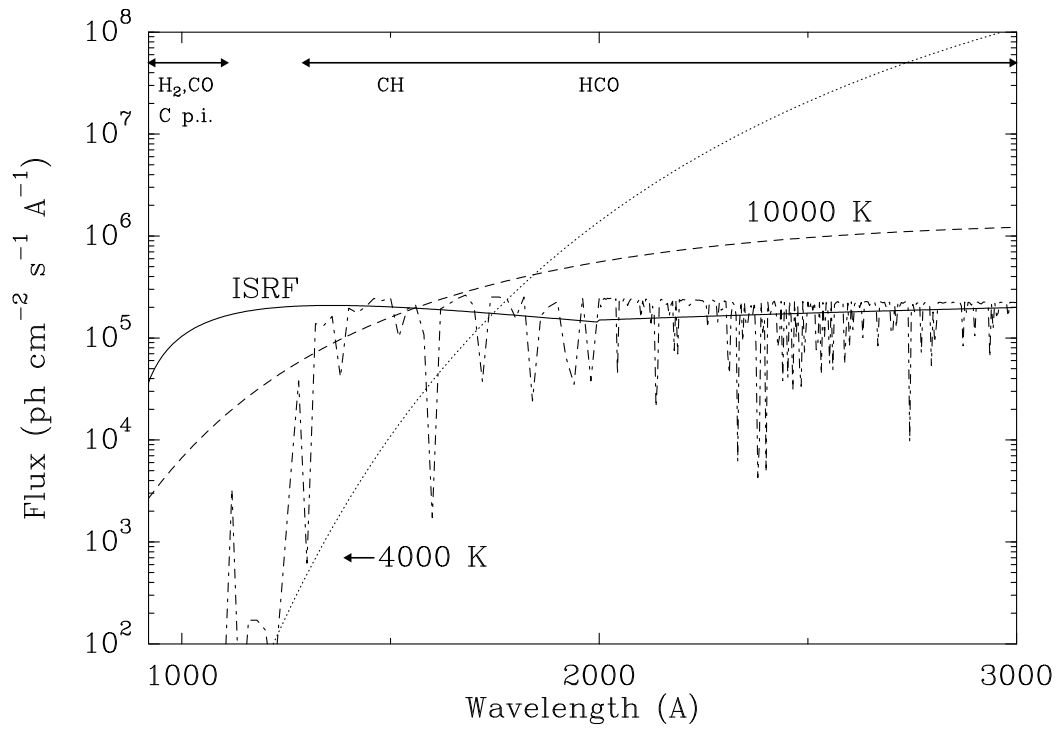


Figure 1: Comparison of the interstellar radiation field (ISRF) according to [12] (with the extension by [74] for $>2000 \text{ \AA}$) with a 10000 K (dashed) and 4000 K (dotted) blackbody scaled to have the same integrated intensity from 912–2050 \AA . The scaled NEXTEGEN model radiation field a B9.5 star [22] (as appropriate for HD 141569A) is included as well (dash-dotted).

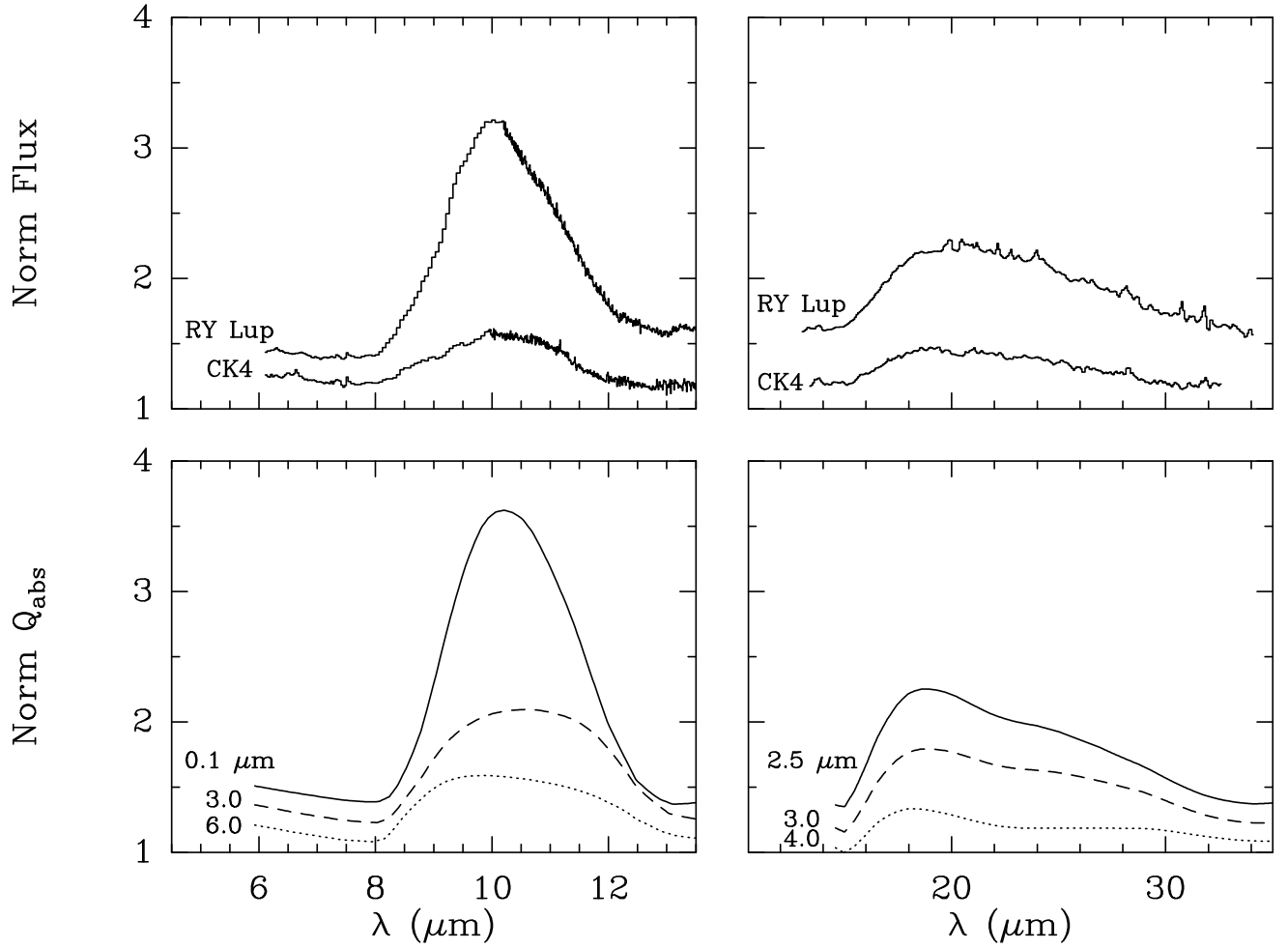


Figure 2: Evidence for grain growth in disks around T Tauri stars. Top: Spitzer Space Telescope observations of the 10 and 20 μm silicate Si-O stretching and O-Si-O bending mode features of two T Tauri stars, shifted by +0.4 and +0.2 for clarity. Bottom: normalized absorption efficiencies Q_{abs} for models of spherical amorphous olivines with various sizes, calculated using the distribution of hollow spheres (DHS) method of [49]. The models are offset by +0.4, +0.25 and +0.1, respectively. Figure based on [32].

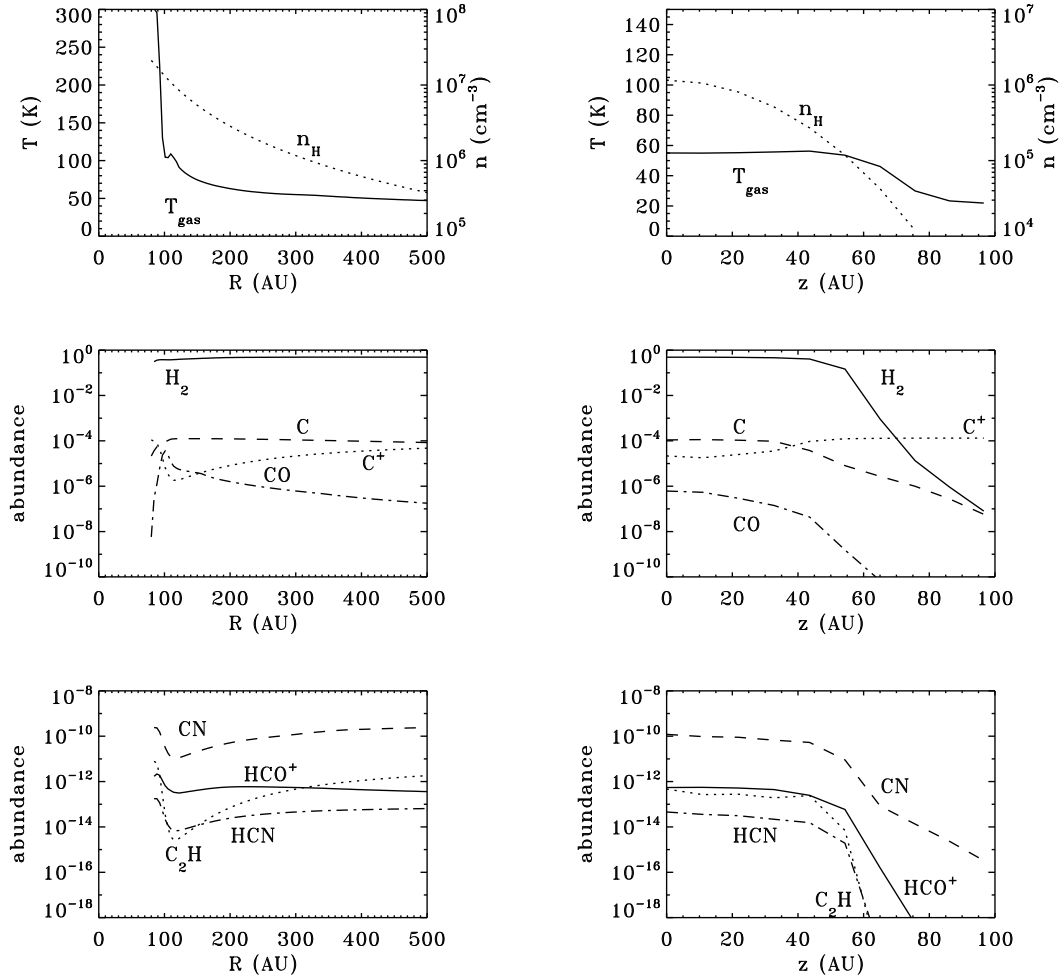


Figure 3: Left: Radial distribution in the midplane of the HD 141569A disk of the temperature and density (top), and various chemical species (middle and bottom). Right: Vertical slice at $R = 300$ AU. This model includes both the stellar radiation (Figure 1) and the ISRF.

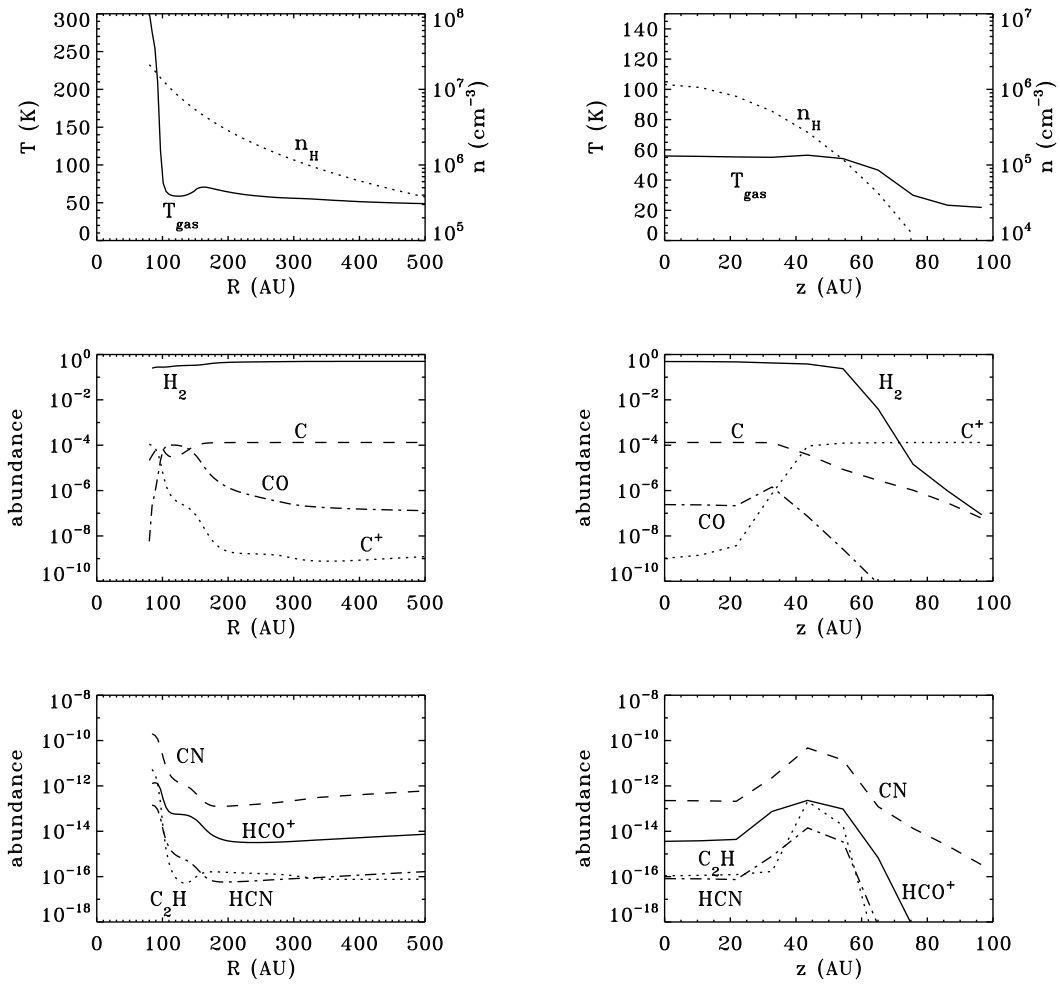


Figure 4: As Figure 3, but without the ISRF.